Remote Sensing of Tropospheric Water Vapor and Cloud Liquid Water by Integrated Ground-Based Sensors

YONG HAN AND E. R. WESTWATER

NOAA/ERL/ETL, Boulder, Colorado

(Manuscript received 24 October 1994, in final form 10 February 1995)

ABSTRACT

A technique is presented for deriving tropospheric water vapor and cloud liquid water, as well as temperature, from a suite of ground-based sensors. Included in the suite are a dual-channel microwave radiometer, a ceilometer, a radio acoustic sounding system (RASS), and conventional surface meteorological instruments. A linear statistical inversion algorithm, combined with a data classification technique, is applied to retrieve water vapor and cloud liquid water profiles. The linear statistical inversion algorithm is also applied to derive temperature profiles from RASS virtual temperature measurements and surface meteorological parameters. A physical retrieval algorithm is then applied to retrieve integrated water vapor and liquid water. Finally, these two algorithms are coupled in a two-step iteration process. The technique is evaluated by comparing retrieved quantities with radiosonde measurements and by comparing this technique with the traditional technique based solely on dual-channel microwave radiometric measurements. Significant improvement is achieved in retrieving dominant structures in the water vapor profile when liquid clouds are present. This evaluation also predicts significant improvement in measuring integrated liquid water, but lack of ground truth prevented experimental verification.

1. Introduction

For many years, most of our knowledge about atmospheric water vapor has been obtained from radiosonde measurements. However, such measurements usually take more than a half hour to complete, during which time the radiosonde balloon may drift several kilometers away from its releasing site. In addition, the quality of radiosonde humidity data is not always reliable, as shown by many studies (Pratt 1985; Wade 1994). Of significant importance is the cost of frequent balloon releases. To supplement or reduce the reliance on radiosondes is a goal shared by many in the remote sensing community.

Over the past decade, there has been considerable effort in development of ground-based remote sensors to measure atmospheric parameters such as wind, temperature, and water vapor. In contrast to the progress made in profiling of wind and temperature by wind profilers and radio acoustic sounding systems (RASS), the ability to measure remotely water vapor profiles is limited. For example, the High-Resolution Interferometer Sounder (HIS) (Smith et al. 1990) provides soundings during clear-air conditions with a vertical resolution of about 200 mb up to about 650 mb; during cloudy conditions its ability to profile vapor is reduced both in range and accuracy. Currently, a very sophisticated Raman lidar (Melfi and Whiteman 1985; Melfi et al. 1989) can measure water vapor with a vertical resolution of 75 m and a temporal resolution of one minute up to about 8.5 km. Its operation is degraded during daytime, and it will not probe through many clouds.

Ground-based microwave radiometers also have been used for water vapor profiling (Skoog et al. 1982; Ruf and Swift 1988). One of the advantages in microwave radiometric observations is the near-all-weather capability. On the negative side, these passive sensors provide only limited information on water vapor profiles. For water vapor profiling, such profile information must be supplied from other sources. A common practice is to apply statistical data to constrain the radiometric inversion (Decker et al. 1978). However, as the constraint is characterized by the conditional mean of the statistical ensemble, vertical resolution of such retrievals is usually poor.

In recent years, new or improved ground-based remote sensors and technologies, such as wind profilers, RASS, cloud radars, and lidars, have become useful in providing additional information to constrain the radiometric inversion. Although the individual sensors may not be able to provide complete water vapor profile information, a combination of the pieces of information from these sensors and the microwave radiometer will yield water vapor profiles with better vertical resolution than those retrieved from a microwave radiometer only. Such a technique to integrate a microwave

Corresponding author address: Yong Han, R/E/ET1, NOAA/ERL/ETL, 325 Broadway, Boulder, CO 80303.

radiometer with other sensors was applied by Westwater et al. (1983) to retrieve temperature profiles from a microwave radiometer and a wind profiler.

In this paper, we present a technique to retrieve water vapor, cloud liquid water, and temperature from the ground using integrated passive, active, and in situ sensors. Included in the package of the sensors were a dual-channel microwave radiometer, a laser ceilometer, a RASS unit, and sensors for measurements of surface pressure, temperature, and humidity. The technique was evaluated by comparisons of retrievals with a year of data from collocated radiosonde measurements. A different retrieval technique has also been applied to similar data obtained during the Winter Icing and Storm Project by Stankov et al. (1995).

2. Instrumentation

The National Oceanic and Atmospheric Administration's (NOAA) Environmental Research Laboratories (ERL) routinely operate a number of remote and in situ sensors at the Stapleton International Airport, Denver, Colorado. Included are a dual-channel microwave radiometer, a 915-MHz RASS unit, and conventional instruments to measure the surface temperature, humidity, and pressure. These sensors are collocated with the National Weather Service (NWS) radiosonde release facility. A cloud ceilometer is also operated by the NWS. Data taken from the above sensors were used for this study. We also used the data from the ERL's 404-MHz RASS unit at Platteville, Colorado, as a supplement to the 915-MHz RASS unit at Denver. Platteville is located about 50 km north of the Denver site. Characteristics and operating parameters of these sensors are summarized in Table 1.

TABLE 1. Instrumental characteristics.

Microwave radiometer (Denver)	
Frequency (GHz)	20.6, 31.65
Bandwidth (double side) (GHz)	1
Sensitivity (K)	0.05
Antenna half-power beamwidth (°)	2.5
Integration time (min)	2
Absolute accuracy (K)	0.5
Ceilometer (Denver)	
Wavelength (nm)	904
Integration time (s)	30
Vertical resolution (m)	15
Measurement range (km)	0–3.6
915-MHz RASS (Denver)	
Profiler frequency (MHz)	915
Vertical resolution (m)	200
RASS acoustic frequency (Hz)	2000
Profiler beamwidth (°)	2
Minimum detectable level (m)	300
RASS acoustic beamwidth (°)	8
404-MHz RASS (Platteville)	
Profiler frequency (MHz)	404
Vertical resolution (m)	320
RASS acoustic frequency (Hz)	900
Profiler beamwidth (°)	4
Minimum detectable level (m)	500
RASS acoustic beamwidth (°)	18
Instruments for surface temperature, humidity, and pressure	
Temperature accuracy (°C)	0.5
Pressure accuracy (mb)	0.5
Relative humidity accuracy (%)	5

a. Dual-channel microwave radiometer

The microwave radiometer is a zenith-viewing instrument that was designed to measure the integrated water vapor and liquid water (Hogg et al. 1983). It contains two independent Dicke-switching-type microwave radiometers operated at 20.6 and 31.65 GHz, respectively. Here we report on radiometric data measured as 2-min averages. Most of the details of the radiometer were contained in Hogg et al. (1983), and new results on the interpretation of the calibration procedure were given by Han et al. (1994a). Although each of the channels has two internal calibration blackbody references, one at temperature 45°C and the other at 145°C, uncertainties that cannot be determined by using the internal references are calibrated out by the so-called tipping curve calibration procedure. This procedure requires measurements at several elevation angles in clear sky conditions so that the sky brightness temperature can be used as a calibration source. The absolute accuracies of the brightness temperature measurements, after "tipping curve" calibration, are estimated, with 99% confidence limits, to be ±0.5 and ±0.9 K for the 20.6- and 31.65-GHz channels (Han et al. 1994a).

b. RASS

RASS is a combination of a wind profiler and an acoustic source. Wind profilers are radio-frequency Doppler radars (915, 404, and 50 MHz are typical frequencies) designed primarily to measure vertical profiles of wind in essentially all weather conditions (Strauch et al. 1987). They detect signals backscattered from turbulence-induced variations of atmospheric refractive index with a spatial scale of one-half the radar wavelength. As the turbulent eddies drift with the wind, the backscattered signals show Doppler frequency shifts, which are proportional to the component of eddy-drifting velocities along the radial direction of the radar beams. Thus, a mean wind vector can be determined by a radar with three or more beams. On RASS operation, an acoustic source generates refractive-index perturbations above a wind profiler by sending pulsed acoustic waves with approximately one-half of the radar's wavelength (May et al. 1989). The vertical beam of a wind profiler measures the ascending speed of the perturbation, which, after correction for vertical wind velocity, is proportional to the square root of the virtual temperature. Thus, RASS measures virtual tempera-

ture profiles with the same vertical resolution as that of the wind profiler.

The 915- and 404-MHz RASS units are designed to operate in two modes. The low mode is used for low-altitude profiling with high vertical resolution; the high mode is used for higher-altitude profiling but with low vertical resolution. The data used in this study are exclusively low mode measurements. The vertical resolutions of the low mode operations are 200 and 320 m, and for the 915- and 404-MHz units, respectively. The height coverage of virtual temperature measurements varies depending on a number of factors, including the atmospheric attenuation of the acoustic waves, which is a function of frequency, temperature, and humidity (May et al. 1989). The 915-MHz RASS unit usually detects virtual temperature up to about 2 km, and the 404-MHz unit up to 4 km. The accuracy of the quality-controlled virtual temperature measurements is generally considered to be better than 1 K. A detailed evaluation of the RASS performance was given by Martner et al. (1993). Because of its superior height coverage, we selected the 404-MHz RASS unit as a reference temperature sensor. However, since the 404-MHz unit was located at Platteville, we used the 915-MHz unit at Denver to provide low-level virtual temperature profiles and extended them to higher levels by adding the measurements from the 404-MHz unit. The temporal resolutions of the virtual temperature data collected for this study were 15, 30, or 60 min.

c. *Laser ceilometer*

A laser ceilometer is designed to measure cloud-base height by detecting the time (and thus, the corresponding distance) needed for a short pulse of light to traverse the atmosphere from the transmitter of the ceilometer to a backscattering cloud base and back to the receiver of the ceilometer. The ceilometer at Denver is operated by the NWS and measures backscattered energy at a wavelength of 904 nm with a temporal resolution of 30 s and a vertical resolution of 15 m. The maximum detectable level of the ceilometer is 3.6 km. The cloud-base height data were conditioned with one of these flags: (a) cloud-base height detected, (b) clear sky, and (c) measurements obscured by fog, precipitation, or other reasons.

d. *Radiosondes and surface meteorological instruments*

The NWS radiosonde balloons are routinely launched every 12 h at standard times. Studies regarding the accuracy of radiosonde soundings have been reported in the literature (Pratt 1985; Wade 1994). Although a number of intrinsic and operational problems of radiosonde soundings are reported in these studies, we used a history of radiosonde data to provide statistical information and contemporary data to provide "ground truth." The radiosonde soundings used were carefully edited to minimize errors.

The microwave radiometer data acquisition system that was used by ERL records measurements of the surface temperature, pressure, and relative humidity. The system operated with a sampling period of 2 min to match the temporal resolution of the microwave radiometer. The accuracies of the surface temperature, pressure, and relative humidity were 0.5°C, 0.5 mb, and 5%. In addition to this system, a commercial moisture sensor was used to indicate if there was precipitation reaching the surface. Data from this sensor helped to eliminate data under raining conditions.

3. Retrieval algorithms

Clouds are often considered as contaminants in radiometric sensing of atmospheric temperature and water vapor. However, the presence of a liquid cloud usually indicates that water vapor in the cloud is at saturation. If we can detect cloud height and measure cloud temperature profiles, water vapor density profiles in clouds therefore can be estimated. In addition, cloud temperature is also an important parameter in deriving integrated cloud liquid water as shown by Westwater (1978) and by Han and Thomson (1994b). Thus, the knowledge of cloud base height and temperature profile can provide substantial information to aid in moisture profile retrievals. Our method derives a complete profile of temperature, water vapor, and cloud liquid from a basic set of measured data: two brightness temperatures, ceilometer-measured cloud-base height, surface meteorological observations, and RASS-measured virtual temperature profiles up to about 4 km. For later use in retrieval of water vapor and cloud liquid water profiles, we extracted from the measured set of data a subset of meteorological parameters—integrated water vapor, integrated cloud liquid, water vapor density at cloud base, and water vapor density at the surface. The vapor density at cloud base was derived from the corresponding RASS temperature, assuming saturation. We used radiometric retrievals of integrated water vapor and liquid water rather than the brightness temperature measurements directly because such a retrieval algorithm can be easily implemented when the integrated water vapor is obtained from other sources, such as the Global Positioning System (GPS) (Rocken et al. 1993). However, GPS does not provide cloud liquid and an independent measurement of this parameter must be obtained. Our method of retrieving profiles is an iterative two-step process. In the first step, we apply a physical retrieval algorithm (Westwater 1978) to derive integrated water vapor and liquid water. In the second step, a linear statistical estimation (Decker et al. 1978) is used to retrieve profiles of temperature, water vapor, and cloud liquid water. Figure 1 illustrates the retrieval process.

a. Physical retrieval of integrated water vapor and liquid water

The integrated water vapor and cloud liquid water were derived by solving the radiative transfer equations at two frequencies ν_1 and ν_2 for two unknowns, the integrated water vapor V and integrated liquid water L, as

$$V = \frac{\bar{K}_{L,\nu_2}\tau'_{\nu_1} - \bar{K}_{L,\nu_1}\tau'_{\nu_2}}{\bar{K}_{V,\nu_1}\bar{K}_{L,\nu_2} - \bar{K}_{V,\nu_2}\bar{K}_{L,\nu_1}}, \quad (1)$$

and

$$L = \frac{-\bar{K}_{V,\nu_2}\tau'_{\nu_1} + \bar{K}_{V,\nu_1}\tau'_{\nu_2}}{\bar{K}_{V,\nu_1}\bar{K}_{L,\nu_2} - \bar{K}_{V,\nu_2}\bar{K}_{L,\nu_1}}, \quad (2)$$

where $\bar{K}_{V,\nu}$ and $\bar{K}_{L,\nu}$ are path-averaged water vapor and liquid water absorption coefficients, respectively. The quantity τ'_ν is the sum of the optical depths of water vapor and liquid water and is derived from the brightness temperature $T_{b,\nu}$ measurements as

$$\tau'_\nu = \ln\left(\frac{T_{mr,\nu} - T_{b,0}}{T_{mr,\nu} - T_{b,\nu}}\right) - \tau_{d,\nu}, \quad (3)$$

where $T_{mr,\nu}$ is the mean radiating temperature, $T_{b,0}$ the external brightness temperature from the "big band" cosmic sources, and $\tau_{d,\nu}$ the dry-air optical depth. Traditionally, the parameters $\bar{K}_{V,\nu}$, $\bar{K}_{L,\nu}$, $T_{mr,\nu}$, and $\tau_{d,\nu}$ are statistically determined and site specific. However, since these parameters are functions of atmospheric state, the use of fixed values for these parameters may cause errors in retrievals. A detailed description and error analysis of (1) and (2) is given by Westwater (1978). Two important error sources in the retrievals of V and L are the uncertainties in estimating the path-averaged liquid water absorption coefficient $\bar{K}_{L,\nu}$ and the mean radiating temperature $T_{mr,\nu}$. These uncertainties are primarily caused by the errors in temperature profile and cloud height. The path-averaged cloud liquid water absorption coefficient is defined as

$$\bar{K}_{L,\nu} = \frac{\int_0^\infty k_{L,\nu}\rho_L dz}{\int_0^\infty \rho_L dz}, \quad (4)$$

where $k_{L,\nu}$ is the mass absorption coefficient of liquid water and ρ_L is the liquid water content. Under the assumption that the cloud drop size lies in the range of Rayleigh approximation, $k_{L,\nu}$ is a function of temperature only. For a given location and season, the variation of $k_{L,\nu}$ is typically about 25%–30% in the middle latitudes (Westwater and Guiraud 1980). A 20%–30% error in L can be induced if incorrect fixed values of $k_{L,\nu}$'s are used. The mean radiating temperature is defined as

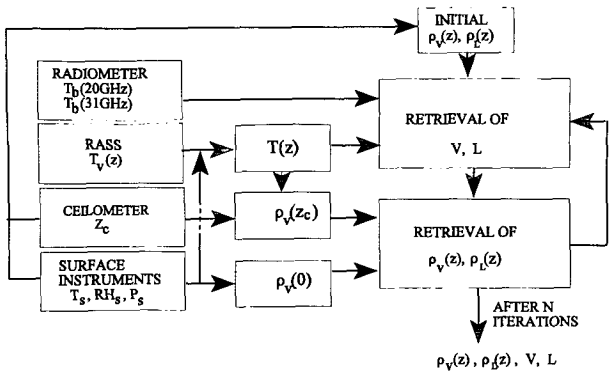

FIG. 1. A schematic diagram of the system to retrieve profiles of temperature $T(z)$, water vapor $\rho_V(z)$ and cloud liquid water $\rho_L(z)$, integrated water vapor V, and integrated cloud liquid water L from measurements of microwave brightness temperatures T_b at 20.6 and 31.65 GHz, virtual temperature profile $T_V(z)$, cloud-base height z_c, and surface temperature T_s, relative humidity RH_s, and pressure P_s; $\rho_V(0)$ and $\rho_V(z_c)$ are water vapor density at the surface and cloud base height, respectively.

$$T_{mr,\nu} = \frac{1}{1 - e^{-\tau_\nu}} \int_0^{\tau_\nu} T(z) e^{-\tau_\nu(z)} d\tau_\nu(z), \quad (5)$$

where $T(z)$ is the temperature profile, τ_ν is the total optical depth of the atmosphere, and $\tau_\nu(z)$ is the optical path between the surface and the height of z. The mean radiating temperature is the average of the temperature profile weighed by the profile of the transmittance, which is modulated by clouds and water vapor. In middle latitudes, the standard deviations of $T_{mr,\nu}$ are typically about 5 K (Westwater and Guiraud 1980). An error of 5 K in $T_{mr,\nu}$ is equivalent to an error of about 0.2 K in brightness temperature measurements under clear sky conditions and an error of about 1 K under cloudy conditions.

In the technique used here, the parameters in (1) and (2) were estimated using a radiative transfer model (Westwater et al. 1990; Han et al. 1994a) and information from available measurements, including inputs of profiles of pressure, temperature, water vapor, and cloud liquid that were obtained from the profile retrievals described in the following section. This approach reduces the error in L significantly.

b. Retrievals of temperature, liquid water, and water vapor profiles

RASS measures virtual temperature $T_V(z)$ over a restricted height range. In addition, recovery of temperature $T(z)$ requires knowledge of the water vapor mixing ratio. In the Denver area the atmosphere is relatively dry, and the virtual temperature near the surface differs from the physical temperature by about 0.4 K in winter and 1.3 K in summer. Although it is possible to couple temperature retrieval with water vapor retrieval through an iterative process, for simplicity

we estimated the water vapor mixing ratio profile from near-surface temperature and humidity measurements by a statistical retrieval process. For locations more humid than Denver, a more elaborate procedure could be used for the virtual temperature correction. We also extrapolated the temperature profile at altitudes above RASS coverage by a statistical regression algorithm that uses the RASS-measured values as predictors (Schroeder 1990).

Profiles of water vapor and cloud liquid water were retrieved through an iteration process. In this process, the profiles retrieved at current step came from the integrated water vapor and liquid water retrieved at previous step. The newly retrieved profiles were used to retrieve the integrated water vapor and liquid water at the next step. The iteration process will be discussed in detail in section 3c. In the following, we describe the profile retrieval algorithm at one of the iteration steps.

To estimate the liquid water profile $\rho_L(z)$, we assumed that the liquid water content was moist adiabatic (Albrecht et al. 1990) and that only one cloud layer is present. Under these assumptions, the cloud liquid content can be calculated from the integrated liquid water L obtained from the microwave radiometer and the cloud temperature profile obtained from RASS.

To retrieve the water vapor profile $\rho_V(z)$, we applied a linear statistical prediction algorithm and chose as linear statistical predictors V, L, and water vapor density $\rho_V(0)$ at the surface level ($z = 0$) and $\rho_V(z_c)$ at cloud-base level z_c. To take advantage of the knowledge of cloud-base height, we also applied a classification procedure. The statistical data were first classified according to cloud-base height. Then the classified inversion coefficients were used to determine the unknown profiles. Specifically, a large collection of radiosonde water vapor profiles, obtained from local climatology, was decomposed into subsets whose members are labeled with the same cloud-base height, within a certain vertical interval Δz. For instance, when the cloud-base height z_c falls within $(i - 0.5)\Delta z$ and $(i + 0.5)\Delta z$, where i is an integer, the profile is classified as a member of subset i. The cloud-base height was assumed to be the lowest level at which the relative humidity exceeded a specified threshold, say 90%.

Two cases were specially treated. When z_c fell below the height of 50 m above the surface, the sounding was considered to be in an environment of precipitation and the profile was consequently not used; when z_c exceeded the maximum detectable level of the ceilometer or no cloud was identified, the profile was classified as "cloud free" with $i = 0$. For each of these subsets, a corresponding set of measurement vectors $\{V, L, \rho_V(0), \rho_V(z_c)\}$ represented by $\{d_j, j = 1, \cdots, m\}$ was generated. Then, a set of regression coefficients $c_j(z = i\Delta z), j = 0, \cdots, m)$ was calculated. The water vapor density $\rho_V(z)$ at height $z = i\Delta z$ is given by

$$\hat{\rho}_V(z) = c_0(z) + \sum_{j=1}^{m} c_j(z) d_j. \tag{6}$$

The a priori radiosonde ensemble, from which the subsets were obtained, contained all NWS radiosonde soundings at Denver from 1970 to 1992. We chose Δz to be 0.25 km, a value that ensured that the sample sizes of the subsets were not too small. When retrieving water vapor profiles, we first used the ceilometer-measured cloud-base height to classify the unknown profile and then applied (6).

We now describe the procedure by which the four-component measurement vectors were prepared for the calculation of regression coefficients c_j. The measurement vectors were simulated from the radiosonde soundings that were used in the regression. The surface water vapor density $\rho_V(0)$ was calculated from radiosonde temperature and relative humidity at the surface level. Gaussian noise levels with the standard deviation of 0.5°C and 5% were added to the temperature and relative humidity, respectively. The water vapor density at cloud base height $\rho_V(z_c)$ was obtained from simulated measurements of RASS temperature and ceilometer cloud-base height. To simulate RASS temperature measurements, we first calculated the virtual temperature from radiosonde data and added 1°C Gaussian random noise. Then, the virtual temperature profile was converted to a physical temperature profile following the procedure described earlier. The integrated water vapor V and liquid water L were derived from simulated microwave brightness temperature measurements using (1) and (2). Brightness temperatures were calculated by using a radiative transfer model (Westwater et al. 1990; Han et al. 1994a) with radiosonde data as inputs and by adding 0.5-K Gaussian random noise. The radiative transfer model included a moist-adiabatic cloud model with a maximum of three layers whose base heights and thicknesses were inferred from radiosonde relative humidity. Thus, although our inverse solution assumes only one cloud layer, our forward model, from which retrieval coefficients were derived, accounts for multilayer clouds. The mean radiating temperature and mass absorption coefficients required by (1) and (2) were calculated from (4) and (5) after first-order temperature, water vapor, and cloud liquid profiles were estimated. The first-order water vapor and cloud liquid profiles are discussed in section 3c. In summary, the output of this portion of the procedure was a set of regression coefficients from which $T(z)$, $\rho_V(z)$, and $\rho_L(z)$ could be estimated from an input data vector. For $T(z)$, the input data are RASS-measured virtual temperature and surface humidity observations. For $\rho_V(z)$ and $\rho_L(z)$, the data vector, for each cloud height interval, is V, L, $\rho_V(0)$, and $\rho_V(z_c)$.

c. *Iteration process*

The iteration process coupled retrievals of water vapor and cloud liquid water profiles with retrievals of

integrated amounts of water vapor and liquid water. We started by deriving initial guesses of water vapor and liquid water profiles. The initial water vapor profiles were derived from the measurements of surface temperature, humidity, and pressure by using a set of regression coefficients. No radiometer data were used in this initial guess. The initial liquid water profiles were assumed to be moist adiabatic. They were constructed by the measurements of the RASS and ceilometer and an arbitrarily specified small amount of integrated liquid. Note that the initial guess profiles were inconsistent if clouds were present but that the inconsistency was removed in subsequent iterations. Using the initial profiles, together with the RASS-measured temperature, we applied a radiative transfer model to calculate the parameters in (1) and (2), by which a first-order approximation to the integrated water vapor V_1 and liquid water L_1 was derived from the brightness temperature measurements. Then, a first-order water vapor profile $\rho_{V,1}(z)$ was calculated using (6) from $\{V_1, L_1, \rho_V(0), \rho_V(z_c)\}$. At the next iteration, the initial water vapor profile was replaced by $\rho_{V,1}(z)$ and the liquid water profile was recalculated using L_1. The process continued until a satisfactory solution was reached. In practice, we terminated the process after the second iteration since little improvement was gained if more iterations were executed.

4. Experimental results

Retrievals of water vapor were evaluated by comparing them with radiosonde soundings. We used both simulated and field measurements for the evaluation. One reason for using the simulated measurements was to achieve a relatively large sample size to make the comparison statistically meaningful. Another reason was that simulation provided the only method readily available to evaluate the retrievals of the integrated liquid water.

a. Retrievals from simulated measurements

The simulated measurements of the microwave radiometer, RASS, ceilometer, and surface meteorological instruments were obtained from radiosondes using the same method as that to generate the simulated measurements for the calculation of regression coefficients as described in section 3b.

We divided the collection of radiosonde data at Denver for the years 1970–92 into dependent and independent sample subsets with a ratio of 2:1. The selections of each individual radiosonde sounding for the subsets were made by using computer-generated random numbers. The dependent subset was used as a training dataset from which the regression coefficients for retrievals were generated, while the independent subset was used for ground truth.

Figure 2 shows examples of retrieved water vapor profiles, compared with radiosondes under cloudy conditions. The retrieved profiles reveal structures that are usually difficult to recover by the traditional technique that used only a microwave radiometer and surface instruments (Decker et al. 1978; Skoog et al. 1982). A statistical evaluation is shown in Fig. 3a, which compares the new retrieval technique with the traditional. We see significant improvement in the retrievals up to about 5 km above the ground. The improvement is attributed to two factors: (a) the water vapor density at cloud level inferred from the combined sensors provided a powerful constraint in retrieving profiles and (b) the classification technique allowed us to apply more height-specific statistical information than with unconstrained retrievals. Figure 3b shows that little improvement was made in retrievals under cloud-free conditions. One reason was that under cloud-free conditions the height constraint at some level above the surface was not applicable. In addition, the benefit of the classification was largely diminished for the data subset conditioned with cloud-free soundings because there was almost no reduction in statistical uncertainty compared to uncertainty from an unclassified data ensemble.

Error analysis also predicts significant improvement in the retrieval of integrated liquid water mainly because of the reduction in error due to estimating the cloud temperature. Table 2 shows statistics of retrieval accuracy for integrated liquid water and water vapor, compared to that using only a dual-channel microwave radiometer with a statistical retrieval algorithm. In general, a 45%–50% improvement in liquid retrieval accuracy was achieved with respect to a statistical inversion algorithm that does not have information on cloud temperature. There is also a slight improvement in retrieval of integrated water vapor under cloudy conditions. The improvement is due to error reduction resulting from estimating mean radiating temperatures, as well as the smaller error due to estimation of cloud absorption coefficients. Note that only the ratio of the two cloud absorption coefficients contributes to V, and the variation of the ratio is much smaller than the variation in the coefficients themselves (Westwater 1978). Note also that although errors caused by an imperfect cloud model were not included in the evaluation, cloud temperature remains an important factor in determining integrated liquid water.

b. Retrievals from observational data

Observational data were collected for the whole year of 1993 at Denver's Stapleton International Airport. Although our sensors were operated continuously, only data from around the radiosonde release time were used in this study. Data in rainy conditions were excluded by checking the moisture sensor operated at the radiometer site. We also rejected data when the brightness temperature measurements at 31.65 GHz exceeded 160 K, a value beyond which the brightness temper-

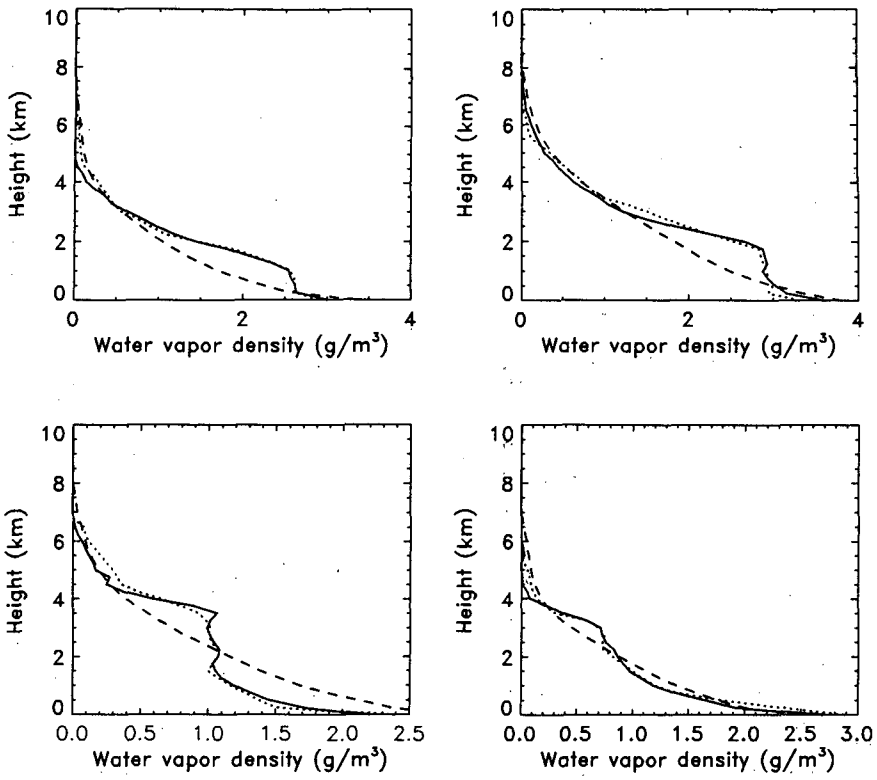

FIG. 2. Examples of retrieved water vapor profiles compared with radiosonde measurements. Simulated measurements were used for the retrievals. Solid line: retrievals by new technique; dashed line: retrievals by traditional technique; and dotted line: radiosonde profiles.

ature measurements were most likely contaminated by rain that contains large liquid droplets that violate the Rayleigh approximation for calculation of cloud absorption coefficients. All remaining data were then carefully screened to remove outliers. Caution was especially exercised in combining data from the two RASS units. Data from the 404-MHz unit were excluded if the overlapping portions of the two virtual temperature profiles disagreed by more than 1 K or, if no overlapping occurred, the region between the two profiles showed large, unrealistic gradients. Fortunately, most of the temperature profiles were combinations of data from the two units.

The radiometer, ceilometer, and surface meteorological data were 2-min averages starting at the radiosonde release time. While an arithmetic averaging was

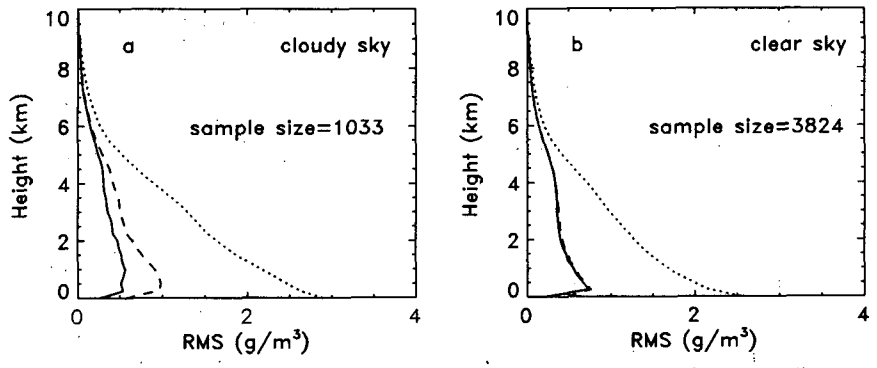

FIG. 3. Root-mean-square differences between retrieved water vapor profiles and radiosonde measurements under (a) cloudy and (b) clear sky conditions. Solid line: new technique; dashed line: traditional technique; and dotted line: variation of radiosonde profiles. Simulated measurements were used for the retrievals.

TABLE 2. Root-mean-square differences between retrievals and ground truth, of integrated water vapor V and liquid water L. A comparison of both physical and statistical retrieval techniques is given. Retrievals of V and L were made from simulated instrumental measurements; the ground truth of V was obtained from radiosondes; the ground truth of L was derived from radiosonde data assuming a moist adiabatic cloud.

	rms V (cm)	rms L (mm)	Sample size
$L > 0.01$ mm			
Physical	0.077	0.051	1033
Statistical	0.092	0.096	1033
$L > 1.00$ mm			
Physical	0.103	0.102	215
Statistical	0.145	0.193	215
$L > 2.5$ mm			
Physical	0.125	0.135	62
Statistical	0.190	0.258	62
Clear sky			
Physical	0.0652	—	3824
Statistical	0.0632	—	3824

used for the other sensors, the averaging algorithm for the ceilometer was the following. There were four ceilometer measurements in 2 min, flagged with "cloud base," "clear sky," or "obscuration." If two or more of the four measurements were flagged with cloud-base, a cloud-base height was determined by taking the mode of the measurements flagged with cloud base. In other cases, if two or more measurements were flagged with obscuration, the data were rejected; otherwise, the 2-min data were conditioned clear sky. The times of the virtual temperature data were confined to within 30 min of the radiosonde release time.

Figure 4 shows examples of retrieved water vapor profiles compared with radiosonde measurements. We see the same features of the retrieved profiles as those appearing in the simulated retrievals. Major profile features were well captured by this retrieval technique, but fine structures were difficult to recover. A statistical evaluation of water vapor profile retrievals under cloudy conditions is shown in Fig. 5.

5. Discussion

In the process of retrieving water vapor profiles, we assumed that water vapor in clouds was saturated. This assumption may not be valid for ice clouds. To ensure the validity of this assumption we required that when clouds were present the microwave radiometer would detect liquid water, and the cloud temperature was above −20°C. In some cases, very thin liquid clouds

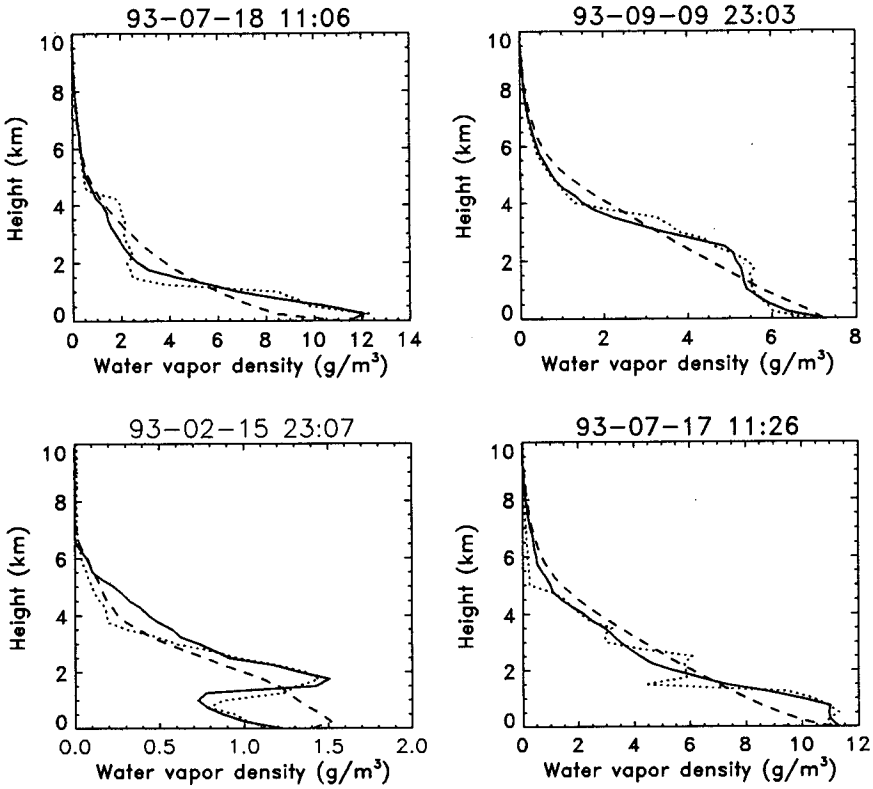

FIG. 4. Examples of retrieved water vapor profiles compared with radiosonde measurements for the data collected at Denver's Stapleton International Airport. Solid line: retrievals by new technique; dashed line: retrievals by traditional technique; and dotted line: radiosonde profiles.

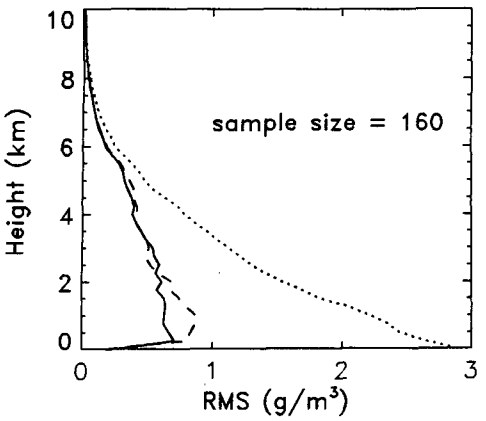

FIG. 5. Root-mean-square difference between retrieved water vapor profiles and radiosonde measurements under cloudy conditions. Solid line: new technique; dashed line: traditional technique; and dotted line: variation of radiosonde profiles.

may be detected by the ceilometer but not by the radiometer. We treated such cases as cloud-free.

To generate regression coefficients and to predict retrieval accuracies, we constructed measurement vectors from our history of radiosonde data by simulation, including simulations of cloud-base height and liquid water content. The cloud-base height was chosen to be the lowest level at which the relative humidity exceeded a specified value. Previous to the deployment of lidar ceilometer by the NWS, it was very difficult to determine what this value should be, since very few soundings indicate a 100% reading in the presence of clouds. Using the 1993 dataset, which does contain ceilometer observations during radiosonde launches, we compared ceilometer cloud-base height measurements with those identified using a fixed threshold relative humidity (RH) criterion. We chose both 90% and 95% as thresholds. When using 95% (Fig. 6b), we found that a large number of ceilometer-measured cloud-base heights corresponded with no-cloud radiosonde profiles or disagreed markedly with "radiosonde cloud base heights." Such discrepancies can be caused by inaccurate or slowly responding radiosonde humidity sensors, balloon drift, or ice clouds. When we lowered the value of the cloud presence criterion to 90% RH, the number of cloudy data pairs increased significantly as shown in Fig. 6a, in comparison with that shown in Fig. 6b. This provided a usable value that allowed us to obtain a reasonable dataset to develop our method. As indicated by the two figures (Figs. 6a, 6b), a 95% criterion is too high to make a significant number of correspondences between ceilometer measurements (assumed correct) and radiosonde measurements (assumed not always representative) of clouds. Our goal is to develop a representative ensemble of clouds, associated with our existing radiosonde data. Since the 90% threshold agreed better with existing data, we adopted it for simulation of cloud base height. In addition, we assumed the cloud liquid water content was moist adiabatic. In reality, moist-adiabatic water content is rarely reached, but studies have shown this is a reasonable approximation (Albrecht et al. 1990).

6. Summary and conclusions

We have presented a technique to derive profiles of water vapor, cloud liquid water and temperature, integrated water vapor, and integrated cloud liquid water from an integrated system of ground-based sensors. Compared with the traditional system of a microwave radiometer and surface meteorological instruments, the new system adds cloud-base height and RASS virtual temperature information that is important for both water vapor and cloud liquid water retrievals. We use a combination of a classification technique and a linear

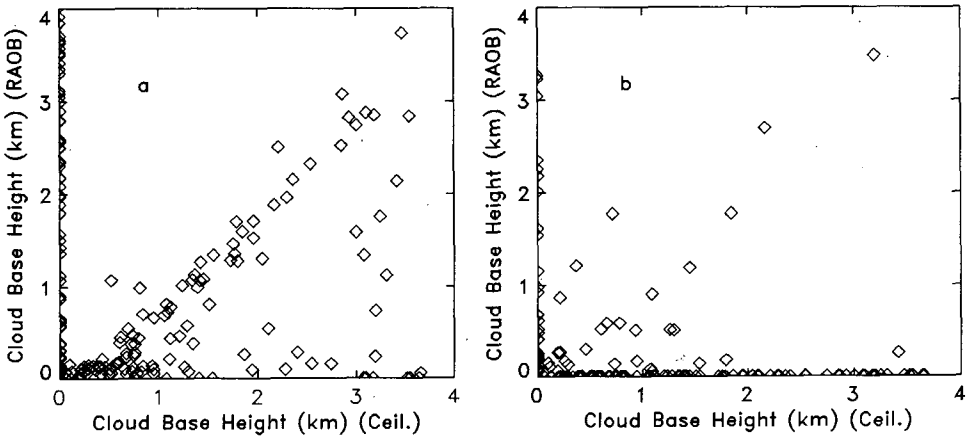

FIG. 6. Comparisons of cloud-base heights measured by a ceilometer and estimated from radiosonde relative humidity profiles, assuming the cloud-base height is the lowest level at which the relative humidity exceeded (a) 90% or (b) 95%.

statistical retrieval algorithm to derive profiles of water vapor, cloud liquid, and temperature and a physical retrieval algorithm to derive integrated water vapor and liquid water. The two retrievals are coupled in an iteration process.

Both simulations and experimental comparisons show that this technique can recover dominant water vapor profile structures under cloudy conditions. The accuracy of water vapor profile retrievals is improved compared to that using the traditional retrieving system. We also predict significant improvement in retrieving integrated cloud liquid. However, no improvement is made in retrievals during clear sky conditions, because then we default to the traditional statistical retrieval algorithm.

One suggestion to improve clear retrievals further is to include measurements of the top of the boundary layer, perhaps defined by the wind profilers. The top of the boundary layers is often associated with large water vapor gradients. In future work, we may include boundary layer height as another variable in the statistical retrievals, similar to the way cloud base height was included in this paper.

Acknowledgments. The authors thank J. B. Snider and M. J. Post for useful comments on the manuscript. This work was partially supported by the Environmental Sciences Division of the Department of Energy as a part of their Atmospheric Radiation Measurement Program.

REFERENCES

Albrecht, B. A., C. W. Fairall, W. H. Schubert, J. B. Snider, D. W. Thomson, and A. B. White, 1990: Surface-based remote sensing of the observed and the adiabatic liquid water content of stratocumulus clouds. *Geophys. Res. Lett.*, **17,** 89–92.

Decker, M. T., E. R. Westwater, and F. O. Guiraud, 1978: Experimental evaluation of ground-based microwave radiometric sensing of atmospheric temperature and water vapor profiles. *J. Appl. Meteor.*, **17,** 1788–1795.

Han, Y., J. B. Snider, E. R. Westwater, S. H. Melfi, and R. A. Ferrare, 1994a: Observations of water vapor by ground-based microwave radiometers and Raman lidar. *J. Geophys. Res.*, **99,** 18 695–18 702.

——, and D. W. Thomson, 1994b: Multichannel microwave radiometric observation at Saipan during the 1990 Tropical Cyclone Motion experiment. *J. Atmos. Oceanic Technol.*, **11,** 110–121.

Hogg, D. C., F. O. Guiraud, J. B. Snider, M. T. Decker, and E. R. Westwater, 1983: A steerable dual-channel microwave radiometer for measurement of water vapor and liquid in the troposphere. *J. Climate Appl. Meteor.*, **22,** 789–806.

Martner, B. E., D. B. Wuertz, B. B. Stankov, R. G. Strauch, E. R. Westwater, K. S. Gage, W. L. Ecklund, C. L. Martin, and W. F. Dabberdt, 1993: An evaluation of wind profiler, RASS, and microwave radiometer performance. *Bull. Amer. Meteor. Soc.*, **74,** 599–613.

May, P. T., and K. P. Moran, 1989: The accuracy of RASS temperature sounding. *J. Appl. Meteor.*, **28,** 19–28.

Melfi, S. H., and D. N. Whiteman, 1985: Observation of lower atmospheric moisture structure and its evolution using a Raman lidar. *Bull. Amer. Meteor. Soc.*, **66,** 1288–1292.

——, ——, and R. A. Ferrare, 1989: Observation of atmospheric fronts using Raman lidar moisture measurements. *J. Climate Appl. Meteor.*, **28,** 789–806.

Pratt, R. W., 1985: Review of radiosonde humidity and temperature errors. *J. Atmos. Oceanic Technol.*, **2,** 404–407.

Rocken, C., R. Ware, T. V. Hove, F. Solheim, C. Alber, J. Johnson, M. Bevis, and S. Businger, 1993: Sensing atmospheric water vapor with Global Positioning System. *Geophys. Res. Lett.*, **20,** 2631–2636.

Ruf, C. S., and C. T. Swift, 1988: Atmospheric profiling of water vapor density with a 20.5–23.5 GHz autocorrelation radiometer. *J. Atmos. Oceanic Technol.*, **5,** 539–546.

Schroeder, J. A., 1990: A comparison of temperature soundings obtained from simultaneous radiometric, radio-acoustic and rawinsonde measurements. *J. Atmos. Oceanic Technol.*, **1,** 495–503.

Skoog, B. G., J. I. H. Askne, and G. Elgered, 1982: Experimental determination of water vapor profiles from ground-based radiometer measurements at 21.0 and 31.4 GHz. *J. Appl. Meteor.*, **21,** 394–400.

Smith, W. L., and Coauthors, 1990: GAPEX: A ground-based atmospheric profiling experiment. *Bull. Amer. Meteor. Soc.*, **71,** 310–318.

Stankov, B. B., B. E. Martner, and M. K. Politovich, 1995: Moisture profiling of the cloudy winter atmosphere using combined remote sensors. *J. Atmos. Oceanic Technol.*, **12,** 488–510.

Strauch, R. G., B. L. Weber, A. S. Frisch, C. G. Little, D. A. Merritt, K. P. Moran, and D. C. Welsh, 1987: The precision and relative accuracy of profiler wind measurements. *J. Atmos. Oceanic Technol.*, **4,** 563–571.

Wade, C. G., 1994: An evaluation of problems affecting the measurement of low relative humidity on the United States radiosonde. *J. Atmos. Oceanic Technol.*, **11,** 687–700.

Westwater, E. R., 1978: The accuracy of water vapor and cloud liquid determination by dual-frequency ground-based microwave radiometry. *Radio Sci.*, **13,** 677–685.

——, and F. O. Guiraud, 1980: Ground-based microwave radiometric retrieval of precipitable water vapor in the presence of clouds with high liquid water content. *Radio Sci.*, **15,** 947–957.

——, M. T. Decker, A. Zachs, and K. S. Gage, 1983: Ground-based remote sensing of temperature profiles by a combination of microwave radiometry and radar. *J. Climate Appl. Meteor.*, **22,** 126–133.

——, J. B. Snider, and M. J. Falls, 1990: Ground-based radiometric observations of atmospheric emission and attenuation at 20.6, 31.65 and 90.0 GHz: A comparison of measurements and theory. *IEEE Trans. Antennas Propag.*, **38,** 1569–1580.